

Spinning Sidebands

The appearance of spinning sidebands in the DAS spectra shown in figure 3.7 leads us directly into a discussion of their location and intensity in NMR experiments. Shown below in figure 3.7 are the slow spinning MAS simulations of both a spin 1/2 and spin 3/2 nucleus. The simulation parameters are identical to figures 2.5 and 2.6, with the

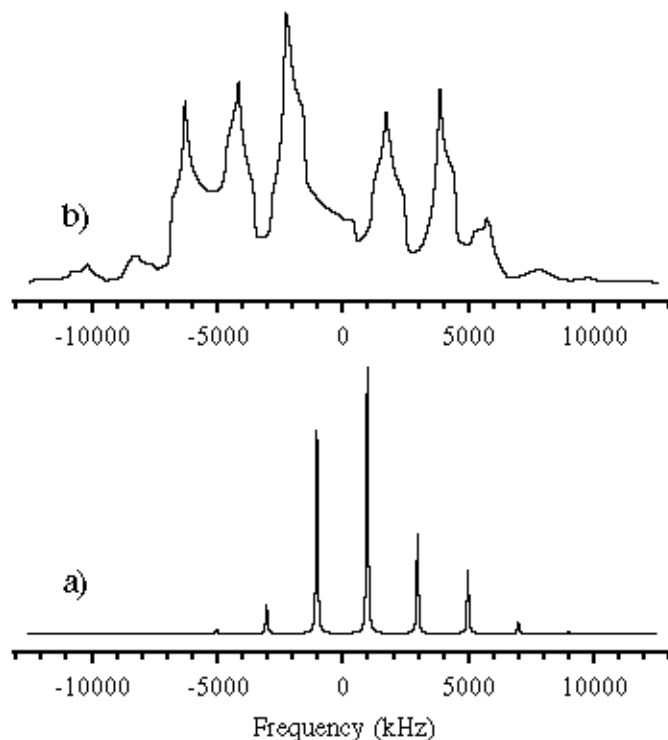


Figure 3.7 Sidebands in MAS Spectra of CSA and Second-Order Quadrupolar Broadened Sites. Simulation parameters were identical to figure 2.5 and 2.6 ($\delta_{iso,CS} = 10$ ppm, $\delta^{CS} = 50$ ppm, $\eta_{CS} = 0.3$ and $C_Q = 3.0$ MHz, $\eta_Q = 0.2$) with the added parameter of a spinning speed of 2.0 kHz.

spinning speed given as 2.0 kHz. It is immediately noticeable that slow spinning produces additional lines not observed in the spectra in figures 2.5 and 2.6. In the case of a spin 1/2 nucleus, the additional spinning sidebands do not significantly hinder interpretation of the spectrum. The only major difficulty in this case comes in integration and identification of the isotropic chemical shift. The integration problem is overcome by adding together the integrated intensity from families of spinning sidebands in the case of multiple sites.⁵⁷ The problem of identifying isotropic sites may be overcome by performing the

experiment at two spinning speeds and the peaks which do not shift will be the isotropic sites. In the case of a spin 3/2 nucleus, the spinning sidebands make the spectrum even more difficult to interpret than in the high speed limit. The sidebands overlap and leave almost no gaps in the overall spectrum. Additionally, the total number of singularities, whose positions normally help to estimate the quadrupolar parameters, is greatly multiplied and cannot be used for this purpose as easily. Finally, in the case of multiple sites, spinning sidebands will make interpretation of quadrupolar spectra virtually impossible.

The source of the spinning sidebands lies in the assumption to drop the time dependent terms from the expressions for the spatial tensor under sample rotation (equation 2.82). This assumption, while simplifying the calculation, in many cases proves to be quite bad. There are a large number of papers in the literature which deal with spinning sidebands. Specifically the works by both Maricq and Waugh⁵⁸ and Herzfeld and Berger⁵⁹ are illuminating for the case of spin 1/2 nuclei. For quadrupolar problems the papers by Jakobsen *et al.*,^{60,61} Samoson *et al.*,^{55,62,63} and others⁶⁴⁻⁷⁶ provide good reference material. For the case of DAS in particular, the papers by Grandinetti *et al.*⁵² and Sun *et al.*⁴⁹ both give a good description of the spinning sideband problem.

To describe spinning sidebands in spin 1/2 systems, it is necessary to return to our original equation for the chemical shift anisotropy energy eigenvalues under spinning conditions.

$$\Delta E^{CSA} = \hbar\omega_I \delta_{isacs} + \hbar\omega_I \delta^{CS} \sqrt{\frac{2}{3}} \sum_{m=-2}^2 \sum_{n=-2}^2 D_{m0}^{(2)}(\omega_r t + \phi_r, \theta, 0) D_{nm}^{(2)}(\alpha^{CS}, \beta^{CS}, \gamma^{CS}) \rho_{2n}^{CS} \quad (3.10)$$

This expression may be written alternatively below

$$\Delta E^{CSA} = \hbar \sum_{m=-2}^2 W_m(\alpha^{CS}, \beta^{CS}, \theta) e^{-im(\omega_r t + \phi_r + \gamma^{CS})}$$

$$W_0(\alpha^{CS}, \beta^{CS}, \theta) = \omega_l \delta_{is\alpha cs} + \sqrt{\frac{2}{3}} \omega_l \delta^{CS} d_{00}^{(2)}(\theta) \sum_{n=-2}^2 e^{-in\alpha^{CS}} d_{n0}^{(2)}(\beta^{CS}) \rho_{2n}^{CS} \quad (3.11)$$

$$W_m(\alpha^{CS}, \beta^{CS}, \theta) = \sqrt{\frac{2}{3}} \omega_l \delta^{CS} d_{m0}^{(2)}(\theta) \sum_{n=-2}^2 e^{-in\alpha^{CS}} d_{nm}^{(2)}(\beta^{CS}) \rho_{2n}^{CS}$$

This expression allows us to write the time domain free induction decay following a pulse.

$$\begin{aligned} \phi^{CS}(t_2) &= \frac{1}{\hbar} \int_0^{t_2} \Delta E^{CSA} dt \\ &= W_0(\alpha^{CS}, \beta^{CS}, \theta) t_2 - \\ &\quad \sum_{m \neq 0} \frac{W_m(\alpha^{CS}, \beta^{CS}, \theta)}{im\omega_r} e^{-im(\omega_r t_2 + \phi_r + \gamma^{CS})} - e^{-im(\phi_r + \gamma^{CS})} \\ S(t_2) &= e^{-i\phi^{CS}(t_2)} \\ &= e^{-iW_0(\alpha^{CS}, \beta^{CS}, \theta)t_2} \\ &\quad \times \exp \sum_{m \neq 0} \frac{W_m(\alpha^{CS}, \beta^{CS}, \theta)}{m\omega_r} e^{-im(\omega_r t_2 + \phi_r + \gamma^{CS})} - e^{-im(\phi_r + \gamma^{CS})} \end{aligned} \quad (3.12)$$

Now we may use Dirac delta functions $\delta(z)$ (see chapter 2) to rewrite 3.12 below.

$$\begin{aligned} S(t_2) &= e^{-iW_0(\alpha^{CS}, \beta^{CS}, \theta)t_2} \\ &\quad \times \frac{1}{2\pi} \int_0^{2\pi} \delta(\psi - \omega_r t_2 - \phi_r - \gamma^{CS}) \exp \sum_{m \neq 0} \frac{W_m(\alpha^{CS}, \beta^{CS}, \theta)}{m\omega_r} e^{-im\psi} d\psi \\ &\quad \times \frac{1}{2\pi} \int_0^{2\pi} \delta(\psi - \phi_r - \gamma^{CS}) \exp \sum_{m \neq 0} \frac{W_m(\alpha^{CS}, \beta^{CS}, \theta)}{m\omega_r} e^{-im\psi} d\psi \end{aligned} \quad (3.13)$$

$$\delta(z) = \frac{1}{2\pi} \sum_{m=-\infty}^{\infty} \exp(-imz)$$

The alternative series expansion definition of delta functions (given in equation 2.90) allows us to write $S(t_2)$ in a different fashion (3.14).

$$\begin{aligned}
S(t_2) &= \exp\left(-iW_0(\alpha^{CS}, \beta^{CS}, \theta)t_2\right) \\
&\times \frac{1}{2\pi} \int_0^{2\pi} \exp\left[iN_1(\psi - \omega_r t_2 - \phi_r - \gamma^{CS}) + \frac{W_m(\alpha^{CS}, \beta^{CS}, \theta)}{m\omega_r} e^{-im\psi}\right] d\psi \quad (3.14) \\
&\times \frac{1}{2\pi} \int_0^{2\pi} \exp\left[iN_2(\psi - \phi_r - \gamma^{CS}) - \frac{W_m(\alpha^{CS}, \beta^{CS}, \theta)}{m\omega_r} e^{-im\psi}\right] d\psi
\end{aligned}$$

This expression may be simplified by reversing the summation over N_2 and pulling the ψ independent terms out of the integrals.

$$\begin{aligned}
S(t_2) &= e^{-iW_0(\alpha^{CS}, \beta^{CS}, \theta)t_2} \sum_{N_1, N_2} A_{N_1} A_{N_2}^* e^{-i(N_1\omega_r t_2 + (N_1 - N_2)(\phi_r + \gamma^{CS}))} \\
A_N &= \frac{1}{2\pi} \int_0^{2\pi} \exp\left[iN\psi + \frac{W_m(\alpha^{CS}, \beta^{CS}, \theta)}{m\omega_r} e^{-im\psi}\right] d\psi \quad (3.15) \\
A_N^* &= \frac{1}{2\pi} \int_0^{2\pi} \exp\left[-iN\psi - \frac{W_m(\alpha^{CS}, \beta^{CS}, \theta)}{m\omega_r} e^{-im\psi}\right] d\psi
\end{aligned}$$

Since all possible crystallite orientations are present in a powder sample, the signal may be simplified by averaging over the $(\phi_r + \gamma^{CS})$ variables.

$$\langle S(t_2) \rangle_{(\phi_r + \gamma^{CS})} = e^{-iW_0(\alpha^{CS}, \beta^{CS}, \theta)t_2} \sum_{N_1=-\infty}^{\infty} A_{N_1} A_{N_1}^* e^{-iN_1\omega_r t_2} \quad (3.16)$$

The final step is to do the powder average over the remaining two Euler angles, $(\alpha^{CS}, \beta^{CS})$ (see section at the end of chapter 2 for a discussion powder averages). In the case of magic-angle spinning, the first exponential term has no orientational dependence, and the signal is given below.

$$\begin{aligned}
\langle S(t_2) \rangle_{MAS} &= e^{-i\omega_l \delta_{iso,cs} t_2} \sum_{N_1=-\infty}^{\infty} S_{N_1} e^{-iN_1\omega_r t_2} \\
S_N &= \frac{1}{4\pi} \int_0^{2\pi} \int_0^\pi |A_N|^2 \sin\beta^{CS} d\beta^{CS} d\alpha^{CS} \quad (3.17)
\end{aligned}$$

This MAS signal shows that there will exist a set of N spinning sidebands a distance $N\omega_r$ from the isotropic peak with intensities given by S_N . In practice, the S_N will die away

fairly quickly with increasing N . In fact, once $N\omega_r$ is outside of the static powder pattern, S_N will be nearly zero (but not absolutely zero). This behavior is seen in the slow speed MAS spectrum for a spin 1/2 nucleus in figure 3.6.

For the case of quadrupolar nuclei, this analysis may again be performed. For the first-order quadrupolar interaction, the math is entirely identical, except that signal must be added together for all of the possible single quantum transitions. The second order quadrupolar interaction presents a more difficult problem. Remember that the expression for the second-order quadrupolar energy splitting is given below (identical to equation 2.97)

$$\Delta E^{(2Q)} = \frac{\hbar\omega_Q^2}{\omega_I} \left(I(I+1) - \frac{3}{4} \right) \left(2A_{21}^Q A_{2-1}^Q + A_{22}^Q A_{2-2}^Q \right) \quad (3.18)$$

This expression may be simplified using the following tensor relationship for products of tensor elements (3.19).

$$\begin{aligned} A_{2m} A_{2-m} &= \sum_{l=0,2,4} \langle l, 0 | 2, 2, m, -m \rangle a_{l0} \\ a_{l0} &= \sum_n D_{n0}^{(l)}(\omega_r t + \phi_r, \theta, 0) \sum_k D_{kn}^{(l)}(\alpha, \beta, \gamma) \sigma_{lk} \\ \sigma_{lk} &= \sum_j \langle l, k | 2, 2, j, k-j \rangle \rho_{2j} \rho_{2k-j} \end{aligned} \quad (3.19)$$

Here the a_{l0} tensor has been explicitly written out for rotation from the PAS to the rotor frame followed by rotation from the rotor frame to the LAB frame. The coefficients $\langle L, M | l, l, m, M-m \rangle$ used in the expansion are the usual Clebsh-Gordon coefficients. For the quadrupolar interaction, this expansion leads to the following formula for the second-order splitting.

$$\begin{aligned}
\Delta E^{(2Q)} &= \frac{\hbar\omega_Q^2}{\omega_l} 2 \left(I(I+1) - \frac{3}{4} \right) \sum_{l=0,2,4} \sum_{m>0} \frac{\langle l,0|2,2,m,-m\rangle}{m} a_{l0}^Q \\
\sigma_{00}^Q &= \frac{3e^2q^2}{2\sqrt{5}} \frac{\eta_Q^2}{3} + 1 \\
\sigma_{20}^Q &= \frac{3e^2q^2}{2} \sqrt{\frac{2}{7}} \frac{\eta_Q^2}{3} - 1, \quad \sigma_{2\pm 2}^Q = \frac{3e^2q^2\eta_Q}{\sqrt{21}} \\
\sigma_{40}^Q &= \frac{9e^2q^2}{\sqrt{70}} \frac{\eta_Q^2}{18} + 1, \quad \sigma_{4\pm 2}^Q = \frac{3e^2q^2\eta_Q}{2\sqrt{7}}, \quad \sigma_{4\pm 4}^Q = \frac{e^2q^2\eta_Q^2}{4}
\end{aligned} \tag{3.20}$$

As previously, we may rewrite the energy splitting in the following fashion (just as in equation 3.10).

$$\begin{aligned}
\Delta E^{(2Q)} &= \hbar \sum_{n=-4}^4 e^{-in(\omega_r t + \phi_r + \gamma^Q)} W_n(\alpha^Q, \beta^Q, \theta) \\
W_n(\alpha^Q, \beta^Q, \theta) &= \frac{\omega_Q^2}{\omega_l} 2 \left(I(I+1) - \frac{3}{4} \right) \sum_{l=0,2,4} \sum_{|l|=|n|} e^{-in(\omega_r t + \phi_r + \gamma^Q)} d_{n0}^{(l)}(\theta) \\
&\quad \times \sum_k e^{-ik\alpha^Q} d_{kn}^{(l)}(\beta^Q) \sigma_{lk}^Q \frac{\langle l,0|2,2,m,-m\rangle}{m}
\end{aligned} \tag{3.21}$$

It is important to note the similarity between this equation and equation 3.11. In fact, the same analysis may be followed to arrive at a very similar result following the average over rotor phase.

$$\begin{aligned}
\phi^Q(t_2) &= \frac{1}{\hbar} \int_0^{t_2} \Delta E^{(2Q)} dt \\
S(t_2) &= e^{-i\phi^Q(t_2)}
\end{aligned} \tag{3.22a}$$

$$\begin{aligned}
\langle S(t_2) \rangle_{(\phi_r + \gamma^Q)} &= e^{-iW_0(\alpha^Q, \beta^Q, \theta)t_2} \sum_{N_1=-} A_{N_1} A_{N_1}^* e^{-iN_1\omega_r t_2} \\
A_N &= \frac{1}{2\pi} \int_0^{2\pi} \exp iN\psi + \sum_{n=0} \frac{W_n(\alpha^Q, \beta^Q, \theta)}{n\omega_r} e^{-in\psi} d\psi \\
A_N^* &= \frac{1}{2\pi} \int_0^{2\pi} \exp -iN\psi - \sum_{n=0} \frac{W_n(\alpha^Q, \beta^Q, \theta)}{n\omega_r} e^{-in\psi} d\psi
\end{aligned} \tag{3.22b}$$

This again shows that all of the sidebands will appear at a frequency $N\omega_r$ from the centerband with positive intensity given by $|A_N|^2$. In this case, the averaging over the final two Euler angles may not be performed analytically, since the second-order quadrupolar frequencies are anisotropic under all single axis spinning angles. The result of a complete powder average is to generate spectra much like the slow speed spin-1/2 MAS spectrum in figure 3.6 except that instead of narrow isotropic lines there will be miniature powder patterns as seen in the same figure. With the above equations, simulations of spinning sidebands may be accomplished with methods similar to those described at the end of chapter 2. There are faster methods, however, for simulating sideband intensities and I would direct the reader to various papers on this and related subjects.^{49,52,58-60,64,74,76-81}

Finally, suppose the spinning angle θ is set to 0° , or parallel to the static magnetic field. In this case, all of the W_n with $n \neq 0$ will be analytically zero for both the chemical shift and quadrupolar interactions. This means that spinning the sample parallel to the magnetic field has absolutely no effect on the spectrum (relative to a static experiment) and generates no spinning sidebands. This feature will be useful in the next section when the $k = 5$ DAS experiment is described, as one of the spinning angles is indeed 0° .

The dynamic angle spinning experiment may be analyzed in a very similar manner as the previous two cases. The first step is to redefine the time axes in the normal DAS experiment. In figure 3.8, the new time definitions are shown along with the original DAS sequence. Notice that the only difference is that the evolution between the first two $\pi/2$ pulses is defined as t_1 rather than $t_1/(k+1)$ and the t_2 evolution begins immediately following the last $\pi/2$ pulse. This definition of time axes differs from the original DAS experiment only in the application of a shearing transformation following the two-dimensional Fourier transform. The shearing angle is related to the k value by the following equation.

$$\theta_s = \tan^{-1} k \quad (3.23)$$

Shearing transformations are well known in NMR⁸²⁻⁸⁶ and will not be discussed at this point. The two dimensional DAS experiment performed with $k = 1$ (37.38° , 79.19°) on

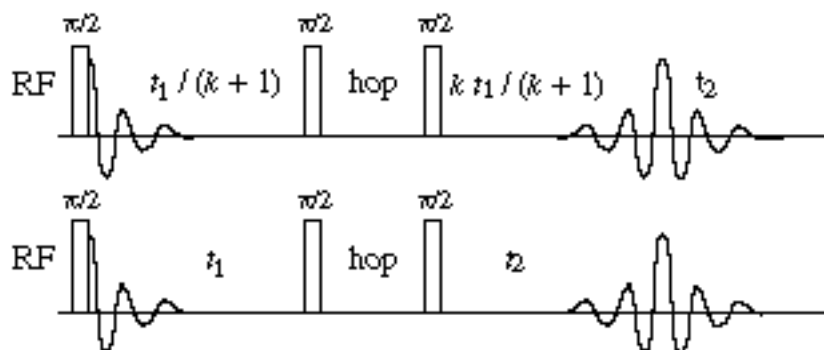


Figure 3.8 Redefined DAS Pulse Sequence for Spinning Sideband Calculation. The time definitions given above are useful for calculating sideband positions and intensities and the original style DAS spectrum may be arrived at by shearing the final two-dimensional Fourier transformed data set.

RbClO_4 is shown in figure 3.9. The $\pi/2$ selective pulse widths were $5.0 \mu\text{s}$ and the spinning speed was 3.2 kHz. The data was taken at a magnetic field strength of 11.7T and was sheared with a 45° shearing transformation. Notice, the shearing transformation creates a spectrum with isotropic peaks and spinning sidebands in the ω_1 (DAS) dimension and anisotropic 79.19° slow spinning VAS spectra in the ω_2 dimension. The positions of the spinning sidebands in the projection onto the ω'_1 DAS axis in figure 3.9 are at the isotropic frequency plus or minus one half the spinning speed. The factor of one half, while initially appearing rather unusual, may be explained by looking at the actual sideband positions with the same formalism used previously.⁵² As a starting point, we will assume that energy splitting will be determined by only the quadrupolar interaction (no CSA present for now, however the results may be easily generalized) given in equation 3.20. In this case the evolved phase may be written as the sum of two integrals, given in equation 3.24.

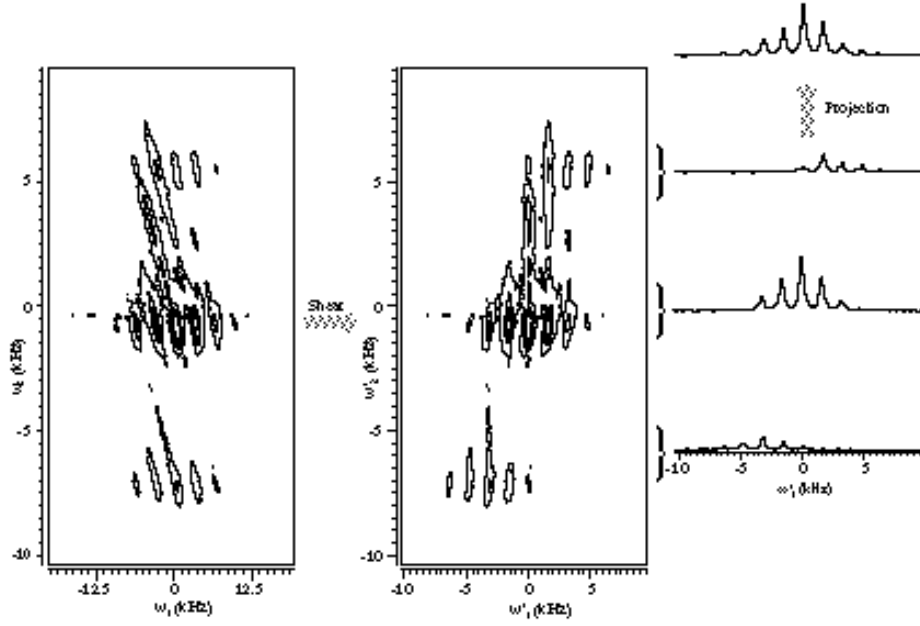


Figure 3.9 Sidebands in $k = 1$ DAS 2D Spectrum of RbClO_4 at 11.7T. The pulse widths were $5.0 \mu\text{s}$ and spinning speed was 3.2 kHz. The data was sheared with a 45° shearing transformation following data collection and processing with the sequence in figure 3.6.

$$\begin{aligned} \phi^{DAS}(t_1, t_2) = & \frac{1}{\hbar} \int_0^{t_1} \Delta E^{(2Q)}(\alpha^Q, \beta^Q, \theta_1, t, \phi_{r1}) dt \\ & + \frac{1}{\hbar} \int_0^{t_2} \Delta E^{(2Q)}(\alpha^Q, \beta^Q, \theta_2, t, \phi_{r2}) dt \end{aligned} \quad (3.24)$$

The variables in the expressions for the energy splitting indicate that we will consider both the absolute rotor phase and PAS orientation of the sample. Upon performing these integrals, the DAS signal may be expressed below.

$$\begin{aligned} \phi^{DAS}(t_1, t_2) = & W_0(\alpha^Q, \beta^Q, \theta) t_1 + W_0(\alpha^Q, \beta^Q, \theta) t_2 \\ & - \sum_{m \neq 0} \frac{W_m(\alpha^Q, \beta^Q, \theta_1)}{i m \omega_r} e^{-im(\omega_r t_1 + \phi_{r1} + \gamma^Q)} - e^{-im(\phi_{r1} + \gamma^Q)} \\ & - \sum_{m \neq 0} \frac{W_m(\alpha^Q, \beta^Q, \theta_2)}{i m \omega_r} e^{-im(\omega_r t_2 + \phi_{r2} + \gamma^Q)} - e^{-im(\phi_{r2} + \gamma^Q)} \end{aligned} \quad (3.25a)$$

$$\begin{aligned}
S(t_1, t_2) &= e^{-i\phi^{DAS}(t_1, t_2)} \\
&= e^{-iW_0(\alpha^\varrho, \beta^\varrho, \theta_1)t_1} e^{-iW_0(\alpha^\varrho, \beta^\varrho, \theta_2)t_2} \\
&\times \exp_{m=0} \frac{W_m(\alpha^\varrho, \beta^\varrho, \theta_1)}{m\omega_r} e^{-im(\omega_r t_1 + \phi_{r1} + \gamma^\varrho)} - e^{-im(\phi_{r1} + \gamma^\varrho)} \\
&\times \exp_{m=0} \frac{W_m(\alpha^\varrho, \beta^\varrho, \theta_2)}{m\omega_r} e^{-im(\omega_r t_2 + \phi_{r2} + \gamma^\varrho)} - e^{-im(\phi_{r2} + \gamma^\varrho)}
\end{aligned} \tag{3.25b}$$

This can again be simplified with the use of delta functions as before to give the following equation for the DAS NMR signal.

$$\begin{aligned}
S(t_1, t_2) &= e^{-iW_0(\alpha^\varrho, \beta^\varrho, \theta_1)t_1} e^{-iW_0(\alpha^\varrho, \beta^\varrho, \theta_2)t_2} \\
&\times \prod_{N_1, N_2, N_3, N_4} A_{N_1}(\theta_1) A_{N_2}^*(\theta_1) A_{N_3}(\theta_2) A_{N_4}^*(\theta_2) \\
&\times e^{-i \frac{(N_1 - N_2 + N_3 - N_4)(\phi_{r1} + \gamma^\varrho) + (N_3 - N_4)(\phi_{r2} - \phi_{r1})}{(N_1 + N_3 - N_4)\omega_r t_1 + N_3\omega_r t_2}} \\
A_N(\theta) &= \frac{1}{2\pi} \int_0^{2\pi} \exp iN\psi + \frac{W_m(\alpha^\varrho, \beta^\varrho, \theta)}{m\omega_r} e^{-im\psi} d\psi
\end{aligned} \tag{3.26}$$

This may be averaged over the initial rotor phase, $(\phi_{r1} + \gamma^\varrho)$, as before.

$$\begin{aligned}
\langle S(t_1, t_2) \rangle_{\phi_{r1}, \gamma^\varrho} &= e^{-iW_0(\alpha^\varrho, \beta^\varrho, \theta_1)t_1} e^{-iW_0(\alpha^\varrho, \beta^\varrho, \theta_2)t_2} \\
&\times \prod_{N_1, N_2, N_3} A_{N_1}(\theta_1) A_{N_2}^*(\theta_1) A_{N_3}(\theta_2) A_{N_1 - N_2 + N_3}^*(\theta_2) \\
&\times e^{-i[(N_2 - N_1)(\phi_{r2} - \phi_{r1}) + N_2\omega_r t_1 + N_3\omega_r t_2]}
\end{aligned} \tag{3.27}$$

In most cases, the relative phase of the rotor $(\phi_{r2} - \phi_{r1})$ between the first and second evolution periods will be relatively random. In the case of large numbers of scans, these variables $(\phi_{r2} - \phi_{r1})$ may be averaged over as well.

$$\begin{aligned}
\langle S(t_1, t_2) \rangle_{\phi_{r1}, \phi_{r2}, \gamma^\varrho} &= e^{-iW_0(\alpha^\varrho, \beta^\varrho, \theta_1)t_1} e^{-iW_0(\alpha^\varrho, \beta^\varrho, \theta_2)t_2} \\
&\times \prod_{N_1, N_2} |A_{N_1}(\theta_1)|^2 |A_{N_2}(\theta_2)|^2 e^{-i[N_1\omega_r t_1 + N_2\omega_r t_2]}
\end{aligned} \tag{3.28}$$

This indicates that the intensity of all of the sidebands in the two dimensional spectrum will be positive. The peaks will occur at frequencies $N_1\omega_r$ from $W_0(\theta_1)$ in the first dimension correlated with frequencies at $N_2\omega_r$ from $W_0(\theta_2)$ in the second. When the spectrum is sheared, the peaks will all remain positive, however their positions will shift. Transforming the time variables into the sheared time definitions, we will arrive at the following expression for the DAS signal.

$$\begin{aligned} t_1 &= \frac{t_1}{k+1} \\ t_2 &= \frac{kt_1}{k+1} + t_2 \end{aligned} \quad (3.29a)$$

$$\begin{aligned} \langle S(t_1, t_2) \rangle &= e^{-i \frac{(W_0(\alpha^Q, \beta^Q, \theta_1) + kW_0(\alpha^Q, \beta^Q, \theta_2))t_1}{k+1}} e^{-iW_0(\alpha^Q, \beta^Q, \theta_2)t_2} \\ &\times \left| A_{N_1}(\theta_1) \right|^2 \left| A_{N_2}(\theta_2) \right|^2 e^{-i \frac{N_1\omega_r t_1}{k+1} + \frac{kN_2\omega_r t_1}{k+1} + N_2\omega_r t_2} \end{aligned} \quad (3.29b)$$

The definition of the DAS angle pairs is equivalent to the following equation.

$$W_0(\alpha^Q, \beta^Q, \theta_1) + kW_0(\alpha^Q, \beta^Q, \theta_2) = (k+1)\omega_{iso}^{(2Q)} \quad (3.30)$$

Which reduces equation 3.29 to the form in equation 3.31.

$$\begin{aligned} \langle S(t_1, t_2) \rangle &= e^{-i\omega_{iso}^{(2Q)}t_1} e^{-iW_0(\alpha^Q, \beta^Q, \theta_2)t_2} \\ &\times \left| A_{N_1}(\theta_1) \right|^2 \left| A_{N_2}(\theta_2) \right|^2 e^{-i \frac{N_1\omega_r t_1}{k+1} + \frac{kN_2\omega_r t_1}{k+1} + N_2\omega_r t_2} \end{aligned} \quad (3.31)$$

$$\langle S(t_1, 0) \rangle = e^{-i\omega_{iso}^{(2Q)}t_1} \left| A_{N_1}(\theta_1) \right|^2 \left| A_{N_2}(\theta_2) \right|^2 e^{-i \frac{N_1}{k+1} + \frac{kN_2}{k+1} \omega_r t_1}$$

This equation shows that the isotropic spectrum arrived at by Fourier transforming the DAS echo tops at $t_2 = 0$ will have sidebands at multiples of two frequencies, $k\omega_r/(k+1)$ and $\omega_r/(k+1)$. The two dimensional spectrum will have sidebands at multiples of the same two frequencies in ω_1 and at ω_r in ω_2 . Looking again at the two dimensional DAS spectrum in figure 3.9 we observe exactly these sideband positions. Each of the slices ex-

tracted on the right corresponds to the isotropic peak and sidebands where $N_1 = 0, \pm 1, \pm 2, \pm 3$, etc for $N_2 = -2, 0$ and $+2$ respectively. It is interesting also that the $N_2 = -1$ and $+1$

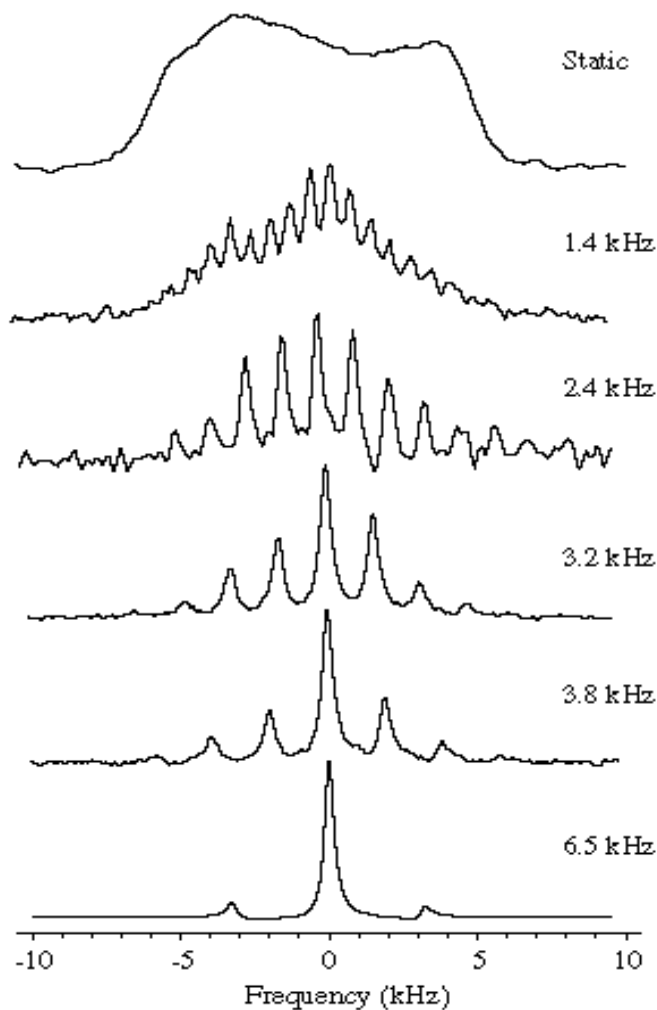


Figure 3.10 1D $^{87}\text{RbClO}_4$ DAS Spectra at a Variety of Spinning Speeds;. The $k=1$ DAS spectra are shown over a range of spinning speeds. The intensity of the sidebands may be described by equation 3.30.

slices have very low intensity as the detection angle (79.19°) is nearly 90° where odd order sidebands may be shown to have no intensity. Also, it may be seen that the most intense peak in each of these slices corresponds to the $N_1 = 0$ peak. The sidebands in each of the slices are separated by $\omega_r/(k + 1)$ which in this case is $\omega_r/2$.

Figure 3.10 shows the one-dimensional DAS spectrum of $^{87}\text{RbClO}_4$ taken at 11.7T at a variety of spinning rates for the usual $k = 1$ case just as in figure 3.9. The sideband intensities are seen to grow more numerous and intense as the spinning speed is reduced. The intensity of each sideband is derived from equation 3.31 by adding together the intensity (see equation 3.33) from each N_1, N_2 pair which contributes an integrated intensity of $\frac{1}{4\pi} \int_0^{2\pi} \int_0^\pi |A_{N_1}(\theta_1)|^2 |A_{N_2}(\theta_2)|^2 \sin\beta^\varrho d\beta^\varrho d\alpha^\varrho$ at a given sideband position $\left(\frac{N_1}{k+1} + \frac{kN_2}{k+1}\right)\omega_r$ from the centerband (keeping in mind that there may be degeneracies when k is an integer). As is the case with double rotation (DOR, see chapter 6), the spinning sideband intensities in DAS do not necessarily approximate the static powder pattern in the limit of very slow spinning as is the case in slow spinning MAS.

When one of the spinning angles is 0° , as in the case of $k = 5$ DAS, the formula for the DAS signal is simplified further. Since all $W_n(0^\circ)$ with $n \neq 0$ are zero, the value of the intensity integrals will be simplified. In the case where θ_1 is 0° , there will be sidebands in the ω_1 dimension of the unshared spectrum and all sideband intensities with $N_1 \neq 0$ will be zero.

$$\begin{aligned} \langle S(t_1, t_2) \rangle_{\phi_{r1}, \phi_{r2}, \gamma^\varrho} &= e^{-i\omega_{iso}^{(2\varrho)} t_1} e^{-iW_0(\alpha^\varrho, \beta^\varrho, \theta_2) t_2} \\ &\times \int_{N_2} |A_{N_2}(\theta_2)|^2 e^{-i \frac{kN_2\omega_r t_1}{k+1} + N_2\omega_r t_2} \quad (3.32) \\ \langle S(t_1, 0) \rangle_{\phi_{r1}, \phi_{r2}, \gamma^\varrho} &= e^{-i\omega_{iso}^{(2\varrho)} t_1} \int_{N_2} |A_{N_2}(\theta_2)|^2 e^{-\frac{ikN_2\omega_r t_1}{k+1}} \end{aligned}$$

A $k = 5$ DAS spectrum is shown below in figure 3.11. The unshared spectrum correlating the static 0° spectrum with the 63.43° VAS spectrum shows that there are no sidebands in the ω_1 dimension and the sidebands are spaced by ω_r in the ω_2 dimension. In the shared spectrum, the sidebands in the DAS dimension are spaced by $5\omega_r/6$ and by ω_r in the anisotropic spectrum. This represents the highest possible effective spinning speed in the isotropic dimension in a DAS experiment.

In a case where the time ratio k (or alternatively $1/k$) is not an integer then the one dimensional isotropic projection becomes more complicated. In the case of a non-integer k , the sidebands at multiples of the two frequencies $k\omega_r/(k+1)$ and $\omega_r/(k+1)$ will not overlap for small integer values of N_1 and N_2 . In the full two dimensional spectrum, the sidebands will appear separated, but will not overlap when projected. This sideband behavior may be seen in the $k = 0.8$ 2D DAS spectrum of RbClO_4 in figure 3.12. Notice also that there are analytically no odd sidebands in the second dimension corresponding

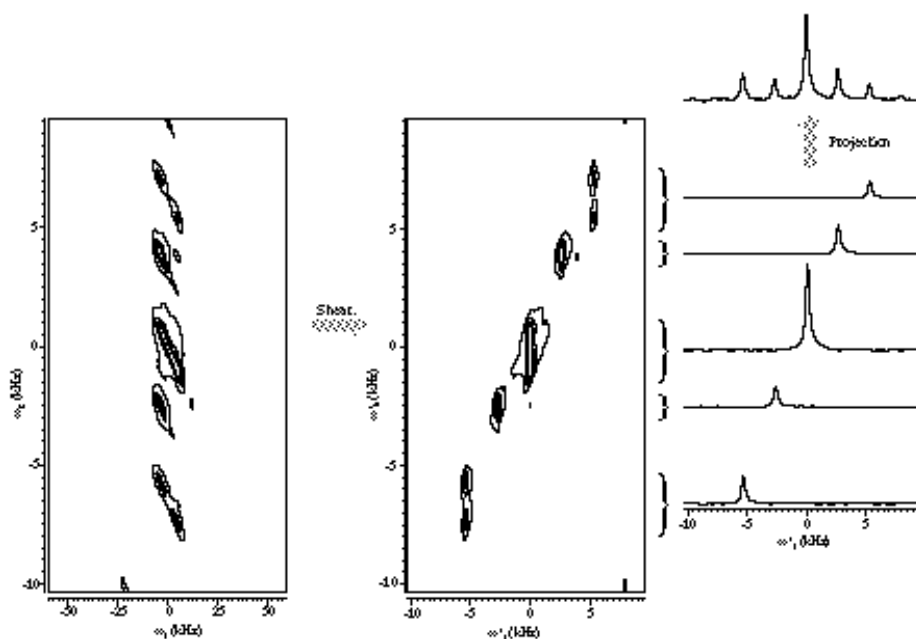


Figure 3.11 $^{87}\text{RbClO}_4$ Sidebands in $k = 5$ DAS 2D Spectrum. The acquisition parameters are identical to those used in figure 3.7, with the exception of the angle pair (0° and 63.43°) used.

to odd N_2 . This is a direct result of spinning at 90° since all odd sidebands disappear in a 1D 90° VAS spectrum.

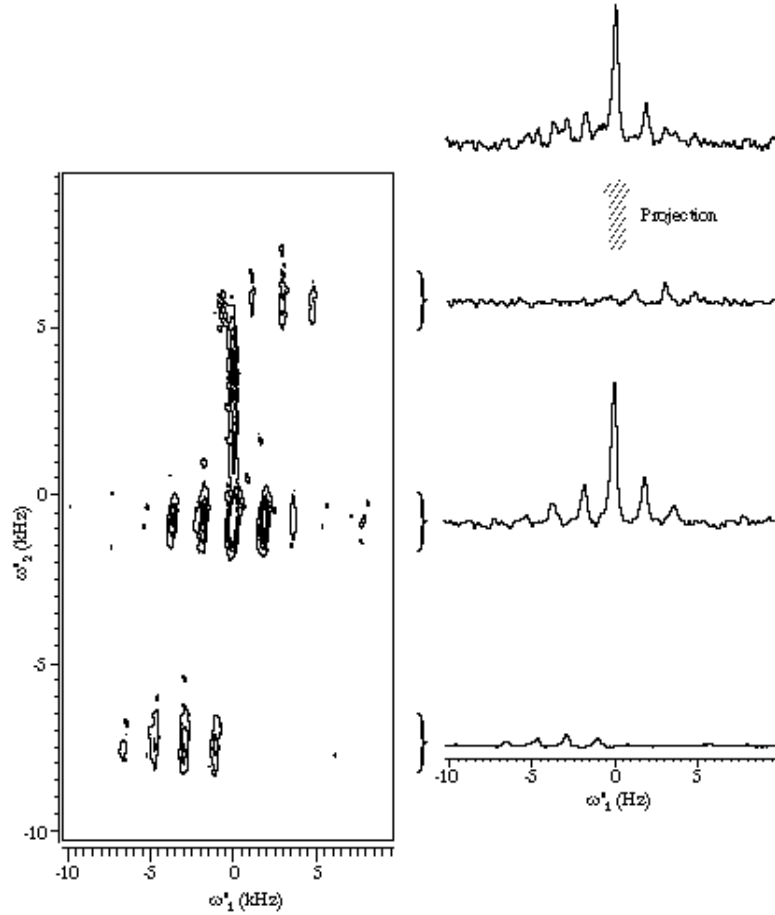


Figure 3.12 $^{87}\text{RbClO}_4$ Sidebands in $k=0.8$ DAS 2D Spectrum. The acquisition parameters again are identical to those used previously, with the exception of the angle pair (39.23° and 90.00°) used.

Returning to the case of one-dimensional DAS projections, the positions of sidebands are given by equation 3.32. This equation may be integrated over the final two powder angles, to yield an expression which may be calculated to generate sideband intensities in a relatively simple manner.

$$\langle S(t_1, 0) \rangle_{\text{powder}} = e^{-i\omega_{\text{iso}}(2Q)t_1} S_{N_1, N_2}(\theta_1, \theta_2) e^{-i \frac{N_1}{k+1} + \frac{kN_2}{k+1} \omega_r t_1} \quad (3.33)$$

$$S_{N_1, N_2}(\theta_1, \theta_2) = \frac{1}{4\pi} \int_0^{2\pi} \int_0^\pi |A_{N_1}(\theta_1)|^2 |A_{N_2}(\theta_2)|^2 \sin\beta^Q d\beta^Q d\alpha^Q$$

This expression was used to calculate spinning sideband intensities for RbClO_4 DAS spectra with k values between 1.0 and 5.0. These simulations are shown next to the experimental spectra in figure 3.13.

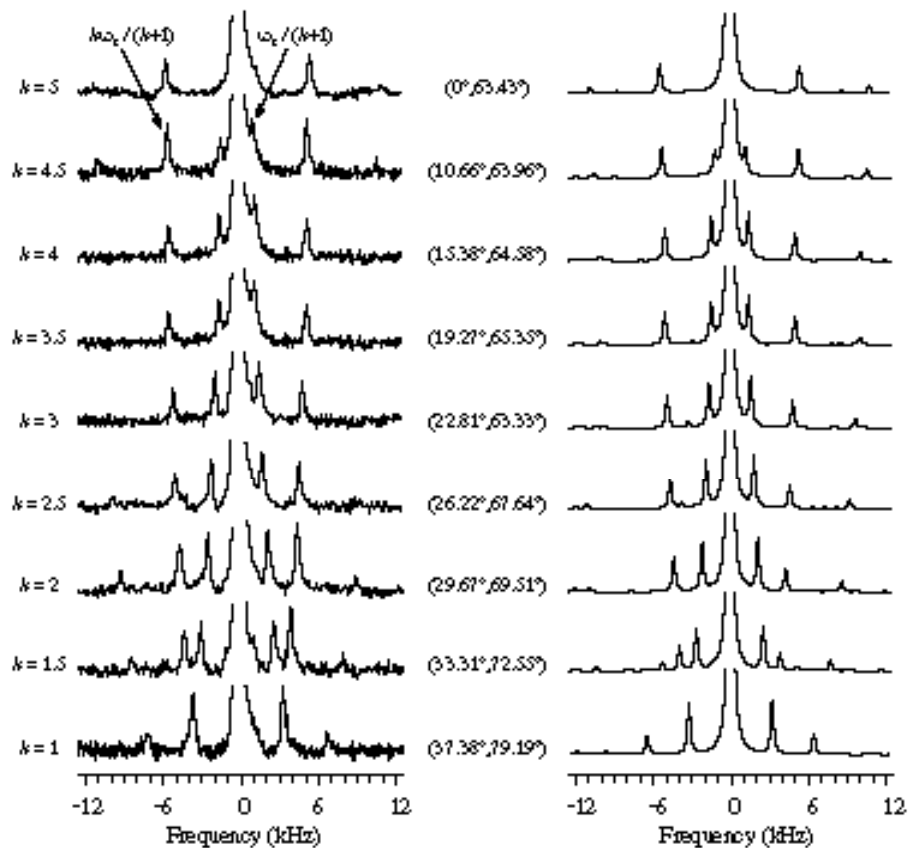


Figure 3.13 All k values for fast spinning $^{87}\text{RbClO}_4$ DAS at 11.7T. These spectra were collected with experimental parameters identical to those used in the previous spectra. The simulated spectra assumed only a quadrupolar coupling C_Q of 3.2 MHz, an asymmetry parameter η_Q of 0.10, ω_r of 6.4 kHz and approximately 300 Hz of Lorentzian broadening.

The quadrupolar parameters used to simulate the spectra were a C_Q of 3.2 MHz, an asymmetry parameter η_Q of 0.10, and a spinning speed ω_r of 6.4 kHz. Lorentzian broadening was added so that the linewidths of simulated spectra were the same as the experimental spectra. It is important to note that there are basically two frequencies of spinning sidebands in these spectra, $\frac{1}{k+1} \omega_r$ and $\frac{k}{k+1} \omega_r$. In the case of $k = 1$, these two frequencies are the same (just as was seen before in figure 3.9) and sidebands appear only at 3.2 kHz. In the case of $k = 5$, the former low frequency sidebands are absent, as predicted by the-

ory and shown earlier in figure 3.11, and only the high frequency 5.3 kHz sidebands appear. Because the spinning speed is quite fast compared to the second-order interaction, only the $N_1 = \pm 1$ or $N_2 = \pm 1$ sidebands appear in these spectra; none of the sum and difference frequencies show up.

In conclusion, the presence of spinning sidebands in DAS spectra can lead to greatly complicated spectra, with multiple spinning frequencies present. By choosing the proper value for the time ratio, $k = 1$ or $k = 5$, the sideband behavior is greatly simplified and the effective spinning speed is maximized. Additionally, the sideband intensities contain information which may be used to extract the quadrupolar coupling parameters. This has not been discussed here and the reader is directed to the thesis of Sun¹⁶ and related papers^{49,52} for additional information on simulating sideband intensities.